EAM
Environmental and Materials
EAM 3(2): 97–113
ISSN 3025-0277

Institute for Advanced Science, Social and Sustainable Future
MORALITY BEFORE KNOWLEDGE

Optimizing vanillin and phenol production from benzyl phenyl ether using $CoMoO_4$/H-ZSM-5: A Box-Behnken design approach

Irena Khatrin[1,2], Duha Rushida Amanullah[1,2], Rahmat Wibowo[1], Russell Francis Howe[3], Yuni Krisyuningsih Krisnandi[1,2,*]

[1] *Department of Chemistry, Faculty of Mathematics and Natural Sciences, Universitas Indonesia, Depok, West Java 16424, Indonesia;*
[2] *Solid Inorganic Framework Laboratory, Department of Chemistry, Faculty of Mathematics and Natural Sciences, Universitas Indonesia, Depok, West Java 16424, Indonesia;*
[3] *Department of Chemistry, School of Natural and Computing Sciences, University of Aberdeen, Aberdeen, Scotland AB24 3UE, United Kingdom.*
*Correspondence: yuni.krisnandi@sci.ui.ac.id

Received Date: July 29, 2025 Revised Date: August 8, 2025 Accepted Date: August 9, 2025

ABSTRACT

Background: Lignin valorization into high-value chemicals is crucial for sustainable development. This study focused on optimizing the catalytic conversion of benzyl phenyl ether (BPE), a lignin model compound, to vanillin and phenolic compounds. **Methods:** Hierarchical H-ZSM-5 was synthesized via a dual-template method and subsequently modified by wet impregnation with bimetallic cobalt and molybdenum oxides ($CoMoO_4$/H-ZSM-5). Catalyst properties were thoroughly characterized using various techniques, including XRD, FTIR, XRF, N_2-physisorption, and SEM-EDS mapping. Reaction conditions, specifically Co:Mo ratio, temperature, and reaction time, were optimized using the Box-Behnken design (BBD), and product yields were quantified by High-Performance Liquid Chromatography (HPLC). **Findings:** Characterization confirmed successful catalyst synthesis, organic template removal, and bimetal oxide incorporation without significant structural damage. Catalytic tests demonstrated 100% BPE conversion. The highest experimental vanillin yield achieved was 54.69%. BBD analysis revealed that the interaction between Co:Mo ratio and temperature, as well as the quadratic effect of Co:Mo ratio, were the most influential factors impacting product yields. The optimal parameters for maximizing vanillin and phenolic yield were determined to be a Co:Mo ratio of 3:7, a temperature of 169 °C, and a reaction time of 31 minutes. While the phenolic model showed a reasonable fit (R^2 = 0.76), the vanillin model exhibited a lower fit (R^2 = 0.34) with significant lack-of-fit. **Conclusion:** This research provides crucial insights into the efficient production of high-value chemicals from BPE, offering a comprehensive optimization approach for the $CoMoO_4$/H-ZSM-5 catalytic system. **Novelty/Originality of this article:** This study represents a novel contribution to lignin valorization.

KEYWORDS: benzyl phenyl ether; vanillin; phenol; $CoMoO_4$/H-ZSM-5; Box-Behnken design.

1. Introduction

Lignin, the second most abundant organic polymer on earth after cellulose, represents an enormous, yet largely underutilized, renewable resource. Despite its widespread presence, the effective implementation of this material as a source for high-value chemicals remains limited. Its complex aromatic structure, interconnected by a high density of strong

Cite This Article:
Khatrin, I., Amanullah, D. R., Wibowo, R., Howe, R. F., Krisnandi, Y. K. (2025). Optimizing vanillin and phenol production from benzyl phenyl ether using CoMoO4/H-ZSM-5: A Box-Behnken design approach. *Environmental and Materials, 3*(2), 97-113. https://doi.org/10.61511/eam.v3i2.2025.2161

ether linkages, particularly the β-O-4 type, renders it highly resistant to degradation (Zeng et al., 2018). Consequently, the efficient cleavage of these resistant C-O ether bonds is identified as an essential step for the successful depolymerization and subsequent conversion into valuable products of lignin biomass.

To fully utilize the vast potential of lignin as a sustainable source for biofuels and fine chemicals, effective depolymerization pre-treatment strategies are essential. Various methods have been explored for lignin depolymerization, including pyrolysis, hydrogenolysis, hydrodeoxygenation (HDO), and microbial degradation (Saini et al., 2022). Among these diverse approaches, hydrodeoxygenation has emerged as one of the most promising and effective catalytic pathways for converting both lignin and model compounds of lignin into high-value chemicals (Jiang et al., 2022). The HDO process typically involves a complex series of simultaneous reactions, such as hydrolysis, dehydration, and dehydrogenation, requiring the use of highly efficient catalysts to aid these multiple conversion steps. Zeolites, particularly ZSM-5, have gained significant attention as highly favored acid catalysts in HDO processes (Luo et al., 2019). The unique properties of these zeolites, including a crystalline aluminosilicate framework, open porous structure with uniform pore sizes, and readily adjustable acidic sites, make them versatile and efficient bases for promoting complex catalytic transformations (Azreena et al., 2021).

Previous studies have explored the application of metal oxides and ZSM-5-based catalysts for converting lignin model compounds. Co_3O_4 has been shown to be effective in the aerobic oxidation of lignin sub-structure compounds such as veratryl alcohol. Its oxygen vacancies can also facilitate the oxidation of lignin-derived compounds under mild conditions, enhancing the breakdown of polymeric chains (Kramer & De Carvalho, 2021; Mate et al., 2014). Furthermore, (Ramadhani et al., 2022) using a Mo-impregnated ZSM-5 catalyst achieved a high conversion rate of diphenyl ether, yielding 7.63% vanillin and 33.32% phenolic compounds. MoO_3-based catalysts are proficient in removing oxygen functionalities from lignin-derived molecules, which is crucial for producing high-value chemicals like vanillin and phenolic compounds (Kohler et al., 2023; Song et al., 2020). The effectiveness of MoO_3 is attributed to its ability to create Brønsted acid active sites for the adsorption and stabilization of reactive intermediates (Zhao et al., 2018). On the other hand, $CoMoO_4$ has been demonstrated to be effective in the conversion of lignin-derived bio-oils and oxygen evolution reactions (Bakhtyari et al., 2020, 2024). The synergy between cobalt and molybdenum in $CoMoO_4$ enhances the catalytic activity by improving electrical conductivity, mass transport, and exposing more active sites. This results in efficient hydrogenation and deoxygenation processes (Wang et al., 2024). More recently, research focusing on the conversion of benzyl phenyl ether, a relevant lignin model compound, using bimetallic CoMo/HZSM-5 (10% loading) demonstrated improved yields, up to 23.3% vanillin and 8.64% phenolic compounds. However, despite these promising initial findings, a thorough and systematic optimization encompassing all critical reaction parameters, such as catalyst composition, loading, substrate-to-catalyst ratio, and reaction temperature for maximizing desired product yields and understanding the interaction of these factors in BPE conversion using CoMo/HZSM-5 has not been adequately addressed. This gap highlights the need for a thorough optimization strategy to unlock the full potential of this catalytic system.

Optimizing chemical reactions involving multiple interacting variables through traditional one-factor-at-a-time methods is often highly inefficient, demanding extensive time and substantial resources. To address these limitations, statistical experimental design methodologies offer robust alternatives. Response Surface Methodology (RSM) stands as a powerful statistical tool widely employed across various fields, including analytical chemistry and chemical engineering, for optimizing complex processes such as transesterification reactions and biodiesel production (Dwivedi & Sharma, 2015). Among the different RSM designs, the Box-Behnken design is particularly advantageous and efficient for experiments involving a moderate number of variables (typically 3 to 5), as it utilizes a three-level factorial basis with strategically selected points, significantly reducing

the number of experimental runs required compared to full factorial designs, thereby saving time and cost (Bezerra et al., 2008).

Therefore, this research aims to synthesize hierarchical porous H-modified ZSM-5 impregnated with bimetallic cobalt and molybdenum oxides ($CoMoO_4$ /HZSM-5), to serve as an effective catalyst for the conversion of benzyl phenyl ether into vanillin and phenolic compounds. To the best of our knowledge, this study represents the first comprehensive investigation utilizing a Box-Behnken design for the simultaneous optimization of key variables in this specific Co-Mo/HZSM-5 catalytic system for BPE conversion. The independent variables selected for optimization include the bimetal ratio (Co:Mo), reaction temperature, and time. Through this systematic and multi-parametric approach, we aim to identify the optimal conditions for maximizing the production of high-value vanillin while concurrently monitoring phenolic compound yields, thereby advancing the efficient conversion to valuable products of lignin model compounds.

2. Methods

2.1 Materials

All chemicals employed in this investigation, including deionized water, were of reagent grade and used without prior purification unless specifically noted. Tetrapropylammonium hydroxide (TPAOH, 40 wt.%), poly(diallyldimethylammonium) chloride (PDDA-Cl, 20 wt.%), tetraethyl orthosilicate (TEOS, 98%), sodium aluminate ($NaAlO_2$), ammonium heptamolybdate tetrahydrate ($(NH_4)_6Mo_7O_{24}{\cdot}4H_2O$), benzyl phenyl ether, and ammonium nitrate (NH_4NO_3) were acquired from Sigma Aldrich. Glacial acetic acid (100%, for analysis), cobalt(II) nitrate hexahydrate ($Co(NO_3)_2{\cdot}6H_2O$), sodium hydroxide (pellets), and ethanol were purchased from Merck.

2.2 Catalyst synthesis and modification

2.2.1 Synthesis of hierarchical ZSM-5

Hierarchical ZSM-5 catalyst was prepared via a hydrothermal method using method from (Pratama et al., 2020) with a molar ratio of $1Al_2O_3$: $64SiO_2$: $10(TPA)_2O$: 3571 H_2O. $NaAlO_2$ and TEOS served as Al and Si sources, respectively. TPAOH directed micropore and MFI structure formation, while PDDA-Cl, a stable cationic polymer, directed mesopore formation (Wang et al., 2010).

The initial synthesis includes dissolving $NaAlO_2$ in distilled water, followed by sequential addition of TPAOH and TEOS, with stirring until homogeneous. The solution pH was then adjusted to ~11 with glacial acetic acid. This mixture was stirred for 3 hours at 100 °C. Subsequently, PDDA-Cl was incorporated and stirred for 48 hours at room temperature. The homogeneous mixture was transferred to a 250 mL Teflon-lined autoclave for crystallization at 170 °C for 144 hours. The resulting product was cooled, washed with demineralized water, filtered, dried overnight at room temperature, and finally calcined at 550 °C for 3 hours to yield the hierarchical ZSM-5, denoted as Z.

2.2.2 Modification of Na-ZSM-5 into H-ZSM-5

H-ZSM-5 was prepared through cation exchange method by dispersing the as-synthesized ZSM-5 in a 1 M NH^{4+} solution prepared by dissolving NH_4NO_3 in distilled water. The resulting mixture was then underwent refluxing and stirring at 60 °C for 6 hours. Following the heating, the mixture was cooled to room temperature, filtered, and subsequently dried at 60 °C. The obtained white powder was then calcined at 550 °C for 6 hours and denoted as H-Z.

2.2.3 Metal oxide impregnation

Catalyst modification was carried out through wet impregnation method, with the variation of loading (wt%) determined using the Box-Behnken design. The preparation of the bimetallic Co-Mo oxide mixture followed the procedure by (Ahmad & Upadhyayula, 2019). $Co(NO_3)_2 \cdot 6H_2O$ and $(NH_4)_6Mo_7O_{24} \cdot 4H_2O$ were separately dissolved in distilled water and stirred for 10 minutes. Both solutions were then mixed and transferred to a spray bottle. The as-synthesized HZSM-5 was placed into an evaporating dish, and the mixed solution was sprayed onto the HZSM-5 gradually until a paste consistency was achieved. The resulting paste was dried at 60 °C and subsequently cooled at room temperature for 24 hours, followed by calcination under air flow at 550 °C for 3 hours. The resulting CoMo-oxide supported H-Z catalysts were then denoted as *x*Co*y*Mo/H-Z, with *x* and *y* as the ratio of Co and Mo out of 10 wt.% metal oxide loading, respectively.

2.3 Characterization method

Following synthesis, the catalysts underwent comprehensive characterization to confirm the successful preparation and to investigate their structural and physicochemical properties. The structural and crystalline nature of the as-synthesized and modified ZSM-5 catalysts were assessed using a PANalytical Empyrean X-ray diffractometer operated at 40 kV and 30 mA, employing Cu Kα radiation (λ = 1.54059 Å) for scans within the 2θ range of 5–70°. Relative crystallinity (RC) was determined by analyzing the intensity of the characteristic peaks within 2θ range of 21–26, in accordance with the ASTM D5758-01 method (Gille et al., 2021; Min et al., 2018). Functional groups and the framework structure of catalyst were identified using an Alpha-Bruker Fourier Transform Infrared (FTIR) spectrometer, employing the KBr pellet technique at a spectral resolution of 4 cm^{-1}. Elemental composition, specifically the content of impregnated metals and their effective dispersion within the catalyst, was ascertained through X-Ray Fluorescence (XRF) analyses, carried out on a PANalytical ϵ1 instrument operating at 50 kV with an Ag radiation source. Surface area and pore characteristics were investigated via N_2-physisorption at 77 K, performed on a Quantachrome Quadrasorb-Evo analyzer. Prior to measurement, samples were degassed at 300 °C. Data analysis was executed using Quantachrome NovaWin – Data Acquisition and Reduction software. The specific surface area was quantified by the Brunauer–Emmett–Teller (BET) method. The surface morphology of samples, including particle size and metal dispersion, was examined using a JEOL JSM-6510LA Scanning Electron Microscopy (SEM) instrument.

2.4 Catalytic test

The conversion of BPE was carried out in a batch reaction involving the addition of substrate and catalyst at a mass ratio of 1:2 (BPE:catalyst) dispersed in ethanol:water 50:50 mixture. An inert atmosphere was established by purging the reactor with N_2 gas (2 bar) at room temperature for 10 min. The reactor was then stirred at 100 rpm until the desired reaction temperature. Once the desired temperature was reached, the stirring speed was increased to 500 rpm for the specified duration. Following the reaction, the autoclave was cooled to room temperature, and the product mixture was filtered. Reaction products were identified and quantitatively determined using High-Performance Liquid Chromatography (HPLC, PG LC210) equipped with a C18 column and mobile phase consisting of methanol:water (80:20) at a flow rate of 1 mL/minute. Analysis was performed at a wavelength of 231 nm, with a total run time of 10 minutes. Phenol, vanillin, and BPE were employed as external standards to construct calibration curves (Fig. S1) for accurate quantitative analysis.

2.5 Optimization of catalytic performance

The Box-Behnken design, an element of the response surface method (RSM), was employed in this study to identify the optimal conditions for the conversion of benzyl phenyl ether to vanillin and phenolic compounds. The investigated parameters and their respective levels were: Co:Mo ratio (as a percentage of the total metal loading, with values of 1, 5, and 9), temperature (with values of 100, 150, and 200 °C), and reaction time (with values of 30, 60, and 90 min). These levels were coded as -1, 0, and +1, respectively. The experimental design encompassed fifteen total treatments, specifically planned to systematically explore the experimental space (Table 1). A second-order polynomial equation was utilized to describe the relationship between the various independent variables and their predicted responses, consistent with established principles of Response Surface Methodology principles (Bezerra et al., 2008; Nazari et al., 2021). A general form of this equation is as follows:

$$Y = \beta_o + \sum \beta_i X_i + \sum \beta_{ii} X_i^2 + \sum \beta_{ij} X_i X_j \quad \text{(Eq. 1)}$$

Here, Y represents the predicted response, β_0 is the intercept (regression coefficient of the model), X_i and X_j denote the independent variables, and β_i, β_{ii}, and β_{ij} are the linear, quadratic, and interaction coefficients, respectively.

Table 1. Box-Behnken design from Response Surface Methodology (RSM) and the observed responses; vanillin and phenolic compounds yield (%)

Std	Variables			Responses	
	Co ratio	Temperature (°C)	Time (min)	Vanillin yield (%)	Phenolic yield (%)
1	1 (–1)	100 (–1)	60 (0)	28.96	6.54
2	9 (+1)	100 (–1)	60 (0)	25.18	0.41
3	1 (–1)	200 (+1)	60 (0)	29.01	2.26
4	9 (+1)	200 (+1)	60 (0)	35.21	11.81
5	1 (–1)	150 (0)	30 (–1)	54.69	1.24
6	9 (+1)	150 (0)	30 (–1)	41.36	0.03
7	1 (–1)	150 (0)	90 (+1)	28.91	9.98
8	9 (+1)	150 (0)	90 (+1)	10.39	2.61
9	5 (0)	100 (–1)	30 (–1)	32.75	1.63
10	5 (0)	200 (+1)	30 (–1)	11.96	3.26
11	5 (0)	100 (–1)	90 (+1)	48.72	2.71
12	5 (0)	200 (+1)	90 (+1)	15.44	1.19
13–15	5 (0)	150 (0)	60 (0)	16.22±3.22	0.32±0.24

3. Results and Discussion

3.1 Catalyst characterizations

The structural and crystalline properties of the as-synthesized ZSM-5 catalysts were assessed by XRD. Figure 1a displays the diffraction patterns of the as-synthesized Z, H-Z, and CoMo-oxide supported H-Z samples. The Z zeolite exhibits characteristic diffraction peaks between 2θ = 7-10° and 2θ = 22-25°, which are consistent with the MFI framework structure as confirmed with JCPDS 44–0003 (Syeitkhajy et al., 2025; Treacy & Higgins, 2007). The absence of other diffraction peaks in the pristine Z indicated the successful synthesis of a pure MFI phase without detectable impurities. Furthermore, the diffraction pattern of H-Z after cation exchange shows no significant change compared to the as-synthesized Z, confirming that the cation exchange process did not disrupt the framework structure of ZSM-5.

The diffraction patterns of CoMo/H-ZSM-5 samples largely retain the characteristic H-Z peaks, indicating that the impregnation of bimetallic oxides did not significantly damage

the structural integrity of the ZSM-5 framework. However, the impregnation of bimetallic CoMo-oxides introduced new diffraction peaks in the CoMo/H-Z diffractograms.

In the 9Co1Mo/H-Z catalyst, characteristic peaks of Co_3O_4 spinel was observed at 2θ = 31.3 and 36.8°, with a peak of $CoMoO_4$ at 2θ = 26.5°, indicating the successful formation of bimetallic oxide $CoMoO_4$. However, since the ratio of Co was 9:1 higher than Mo, the creation of Co_3O_4 was inevitable. This prominent formation of Co_3O_4 was expected due to the significantly higher Co:Mo ratio (9:1). The XRD pattern of 5Co5Mo/H-Z exhibited new characteristic peaks of Co_3O_4 (2θ = 36.8°, JCPDS 42-1467) (Liu et al., 2022), MoO_3 (2θ = 25.7, 27.3, 33.7, 39.0, 49.2, 55.2, 57.7, and 58.8°, JCPS 05-0508) (Moravvej et al., 2023), and $CoMoO_4$ (2θ = 26.5°, JCPDS 00-021-0868) (Gamal et al., 2020). The presence of Co_3O_4 and MoO_3 alongside $CoMoO_4$ indicates that even a balanced Co:Mo ratio did not exclusively yield a pure bimetallic CoMoO4 phase, which might be related to the conditions during the calcination process. Similar to 9Co1Mo/H-Z, the 1Co9Mo/H-Z catalyst, with a higher ratio of Mo loading, resulted in the formation of MoO_3 in addition to $CoMoO_4$. The analysis of relative crystallinity was also carried out with Z catalyst exhibited the highest intensity, thus serving as a reference with 100% relative crystallinity. A noticeable decrease in peak intensity and a slight shift in the diffractogram pattern of CoMo/H-ZSM-5 compared to the pristine H-Z are observed, indicating a reduction in the degree of crystallinity after metal impregnation (Nada & Larsen, 2017).

Functional groups and the framework structure of the catalyst were identified by Fourier Transform Infrared (FTIR) spectroscopy. Fig. 1b illustrates the IR spectra of Z before (Z BC) and after (Z AC) calcination. Prior to calcination, absorption peaks were observed at approximately 2980 cm^{-1} and 1467 cm^{-1}, corresponding to the C–H stretching and bending vibrations, respectively. These peaks indicate the presence of the Organic Structure Directing Agents (OSDAs), TPAOH, and PDDAM (Al-Jubouri, 2020). The complete disappearance of these two absorption peaks after calcination confirms the successful removal of the organic templates during the calcination process. Following the cation exchange process of H-form modification using ammonium, two N–H peaks at 3145 and 1387 cm^{-1} disappeared after a calcination process highlighting the successful modification of H-Z catalyst (Asghar et al., 2020).

Absorption peaks within the 3750–3000 cm^{-1} range are indicative of stretching vibrations from silanol (Si–OH) groups. All catalysts reveal two distinct peaks at 3630 and 3440 cm^{-1}, suggesting the coexistence of both isolated and hydrogen-bonded silanol groups, respectively (Sabarish & Unnikrishnan, 2017). The peak at 3440 cm^{-1} may also be attributed to Al–OH groups residing within the Z framework, acting as Brönsted acid sites. Furthermore, characteristic peaks at 1075–1250 cm^{-1} indicate asymmetric T–O stretching, and at 700–850 cm^{-1} indicate symmetric T-O stretching (Kostyniuk et al., 2020). A distinct absorption peak at approximately 549 cm^{-1} (related to DDR5, as labeled in Figure 1b) is characteristic of the double five-membered ring structure found in pentasil zeolites like Z (Luo et al., 2017; Serrano et al., 2014).

The FTIR spectra of CoMo/H-ZSM-5 samples (Figure 1b) further confirm the successful impregnation of metal oxides, showing new absorption peaks in the fingerprint region. Specifically, new peaks at 953 cm^{-1} showing a distorted MoO_4 vibrational mode in $CoMoO_4$, and at 628 cm^{-1} associated with the Mo–O vibrational mode in $CoMoO_4$ (Prasad et al., 2023). New absorption peaks are also seen at 550 cm^{-1} and 564 cm^{-1} indicating characteristic absorptions of MoO_3 (Pan et al., 2022). Characteristic absorption peaks for the Co–O vibrational mode in Co3O4 are also seen at 661 cm^{-1} and 588 cm^{-1} (Fan et al., 2023; Kumar et al., 2019). The appearance of these specific metal oxide vibration bands in the FTIR spectra provides strong corroborating evidence for the successful incorporation of bimetallic Co–Mo species into the Z framework, as observed from XRD analysis.

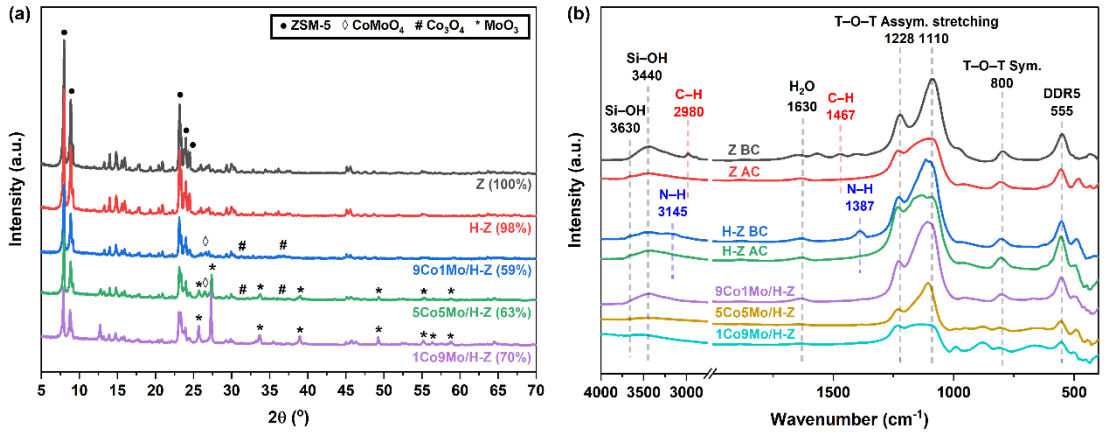

Fig. 1 (a) XRD patterns; (b) FTIR spectra of the as-synthesized and modified ZSM-5 catalysts

XRF results in Table 2 provided insight into the elemental composition. The pristine Z and H-Z catalysts exhibited Si/Al ratios of 64 and 55, respectively. Upon bimetallic CoMo incorporation, the Si/Al ratio decreased for all modified catalysts: 42 for 9Co1Mo/H-Z, 46 for 5Co5Mo/H-Z, and 48 for 1Co9Mo/H-Z. This decrease suggests an alteration in the zeolite framework composition due to the modification process. The actual metal loadings, measured by XRF, confirmed successful Co and Mo deposition onto the H-Z support. Specifically, Co loadings were 28% for 9Co1Mo/H-Z, 11% for 5Co5Mo/H-Z, and 2% for 1Co9Mo/H-Z, while Mo loadings were 11% for 9Co1Mo/H-Z, 42% for 5Co5Mo/H-Z, and 50% for 1Co9Mo/H-Z. The calculated Co:Mo ratios by XRF were 7:3 for 9Co1Mo/H-Z, 2:8 for 5Co5Mo/H-Z, and 0.4:9.6 for 1Co9Mo/H-Z. A discrepancy was observed between the nominal Co:Mo ratios and the ratios measured by XRF. This difference is likely due to the wet impregnation method and the differing affinities of the cobalt and molybdenum precursors for the zeolite support. The higher Mo content in the XRF results for catalysts with higher nominal Mo ratios could indicate a stronger interaction or more efficient deposition of molybdenum species onto the H-ZSM-5 surface compared to cobalt species, which is a plausible explanation for the discrepancy.

N_2-physisorption analysis, specifically the BET method, was used to determine the specific surface area (S_{BET}) of the catalysts. From Table 2, both pristine Z and H-Z exhibit an S_{BET} of 358 $m^2\ g^{-1}$. Upon bimetallic CoMo impregnation, a general decrease in S_{BET} was observed for all modified catalysts. The S_{BET} values were 305 $m^2\ g^{-1}$ for 9Co1Mo/H-Z, 246 $m^2\ g^{-1}$ for 5Co5Mo/H-Z, and 210 $m^2\ g^{-1}$ for 1Co9Mo/H-Z. This reduction in surface area is typically attributed to the deposition of metal oxide nanoparticles onto the zeolite surface and potentially the partial blockage of zeolite pores by these particles (Keluo et al., 2018).

Table 2. Compositional and textural properties of the as-synthesized and modified ZSM-5 catalysts

Catalyst	XRF				N_2-physisorption
	Si/Al	Co	Mo	Co:Mo	S_{BET} ($m^2\ g^{-1}$)
Z	64	-	-	-	358
H-Z	55	-	-	-	358
9Co1Mo/H-Z	42	28	11	7:3	305
5Co5Mo/H-Z	46	11	42	2:8	246
1Co9Mo/H-Z	48	2	50	0.4:9.6	210

The surface morphology and microstructure of the as-synthesized H-Z catalyst and its bimetallic CoMo-derivatives were examined using Scanning Electron Microscopy (SEM), as shown in Figure 2. Figure 2a displays the morphology of the pristine H-Z catalyst, which exhibits distinct particles with relatively smooth surfaces. Upon bimetallic CoMo impregnation, noticeable changes in surface morphology were observed across all modified catalysts (Figure 2b-d). The 1Co9Mo/H-Z (Figure 2b), 5Co5Mo/H-Z (Figure 2c), and 9Co1Mo/H-Z (Figure 2d) catalysts all showed increased surface roughness and the appearance of deposited material on the zeolite surface compared to the parent H-Z catalyst

(Zhu et al., 2013). These visual alterations suggest the successful deposition of bimetallic CoMo-oxides onto the zeolite surface. However, due to the limitations of SEM alone in distinguishing the precise chemical nature and uniform distribution of the deposited bimetal oxides, it was challenging to definitively confirm the successful deposition of these species solely from SEM images. Therefore, further analysis using Energy Dispersive X-ray Spectroscopy (EDS) mapping was performed to ascertain the successful deposition and distribution of the bimetallic oxides.

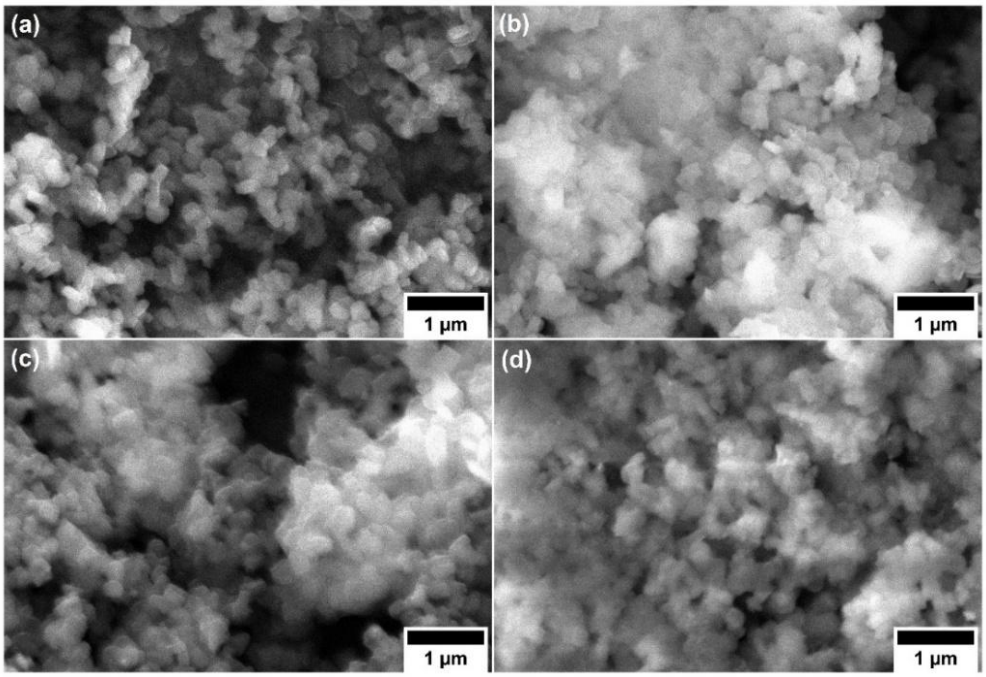

Fig. 2. SEM images of (a) H-Z; (b) 1Co9Mo/H-Z; (c) 5Co5Mo/H-Z; (d) 9Co1Mo/H-Z (20,000x magnification

Energy Dispersive X-ray Spectroscopy (EDS) mapping was employed to further ascertain the successful deposition and spatial distribution of Co and Mo species on the catalyst surface, as illustrated in Figure 3. The EDS mapping presents the distribution of Co (red signal) and Mo (green signal) for catalysts with different Co:Mo ratios. For the 1Co9Mo/H-Z catalyst (Figure 3a), the EDS mapping clearly showed a predominant and relatively uniform distribution of Mo across the catalyst surface, consistent with its high Mo content. In contrast, the Co signal was very sparse and scattered, reflecting its low concentration. Conversely, the 9Co1Mo/H-Z catalyst (Figure 3c), with its high Co content, exhibited a widespread and intense distribution of Co, indicating good dispersion of cobalt species. The Mo signal was minimal and dispersed, aligning with its low Mo ratio. The 5Co5Mo/H-Z catalyst (Figure 3b), representing a more balanced Co:Mo ratio, showed a more co-distributed pattern for both Co and Mo signals. However, both metals appeared with some localized hotspots or brighter areas, suggesting a tendency for slight aggregation or uneven dispersion compared to the more dominant metal in the other two catalysts (Gamal et al., 2020).

Overall, the EDS mapping confirmed the successful deposition of both Co and Mo species onto the H-Z support, with their relative concentrations directly reflecting the nominal Co:Mo ratios. This analysis complements the SEM observations by providing elemental evidence for the presence and distribution of the bimetallic oxides on the catalyst surface.

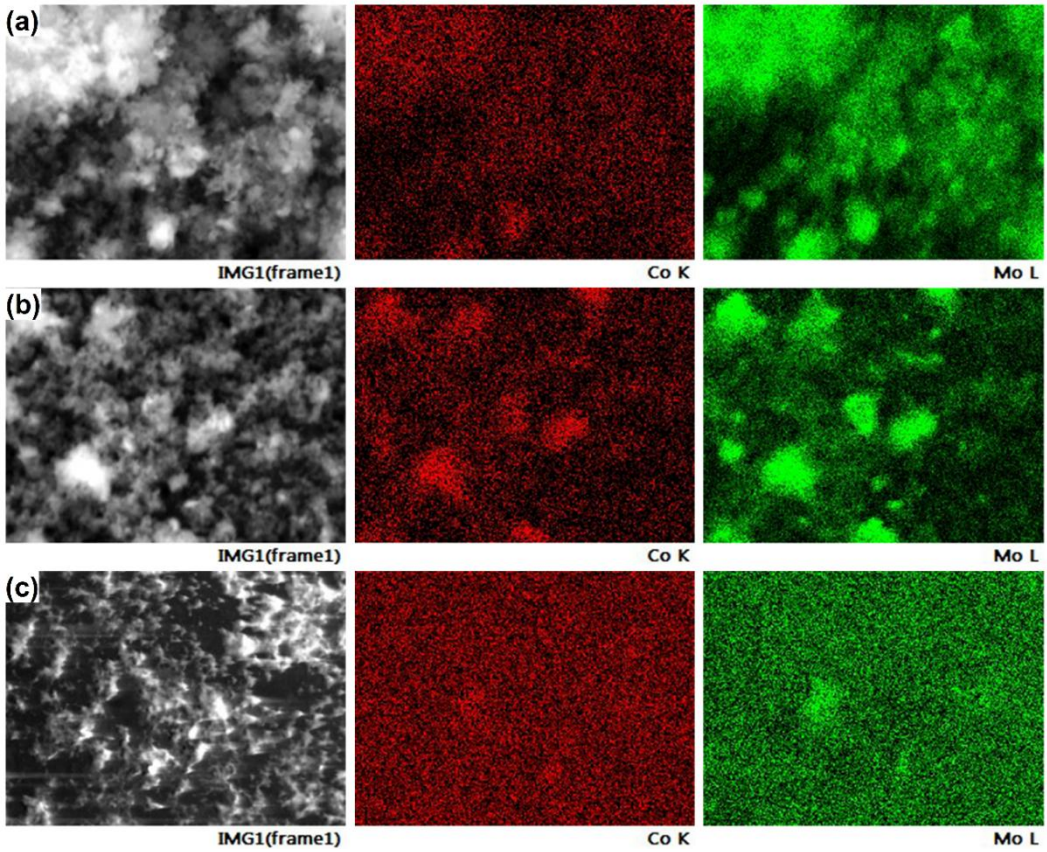

Fig. 3. EDS mapping of Co and Mo of (a) 1Co9Mo/H-Z; (b) 5Co5Mo/H-Z; (c) 9Co1Mo/H-Z

3.2 Catalytic test and optimization

The catalytic conversion of benzyl phenyl ether to vanillin and phenolic compounds was systematically optimized using the Box-Behnken design. In this study, the design incorporated three independent variables: Co:Mo weight ratio (A), Reaction temperature (B), and Reaction time (C). Each variable was tested as three coded levels: low (−1), moderate (0), and high (+1) (El-Sheekh et al., 2024). The experimental matrices, comprising 15 runs, are described in Table 3. The experimental results show 100% BPE conversion, while the yields of vanillin and phenolic compounds are presented in Table 1. The highest yield of vanillin was observed to be 54.69% with a 1:9 Co:Mo ratio (1Co9Mo/H-Z) at 150 °C for 30 minutes. Meanwhile, the highest yield of phenilic compounds was observed to be 11.81% with a 9:1 Co:Mo ratio (9Co1Mo/H-Z) at 200 °C for 60 minutes. These results indicate a strong influence of the Co:Mo ratio on the selectivity of the catalytic reaction. Specifically, the highest vanillin yield (54.69%) was achieved with a 1:9 Co:Mo ratio (1Co9Mo/H-Z), suggesting that a higher molybdenum content favors vanillin production. In contrast, the highest phenolic compound yield (11.81%) was obtained with a 9:1 Co:Mo ratio (9Co1Mo/H-Z), indicating that a higher cobalt content promotes the formation of phenolic compounds.

Table 3. The matrix of BBD optimization

Variables	Symbol	Unit	Range and levels		
			−1	0	+1
Co ratio in CoMo-oxide	A	%	1	5	9
Temperature	B	°C	100	150	200
Time	C	min	30	60	90

This difference in product selectivity can be attributed to the distinct catalytic roles of the metal oxides. The characterization data showed that the 9Co1Mo/H-Z catalyst predominantly contained Co_3O_4 alongside some $CoMoO_4$, while the 1Co9Mo/H-Z catalyst

showed the formation of MoO_3 in addition to $CoMoO_4$. These different phases likely possess varying catalytic activities and selectivity for the reaction pathways. The interaction between the Co:Mo ratio and temperature was identified as the most influential factor on both product yields, highlighting the complex interplay of catalyst composition and reaction conditions.

Table 4. ANOVA test for the yield of vanillin using the quadratic response surface model

Source	Sum of squares	Degree of freedom	Mean square	F-value	p-value	Significance
Model	1154.76	9	128.31	0.46	0.86	not significant
A-Co Ratio	108.27	1	108.27	0.38	0.56	
B-Temperature	241.89	1	241.89	0.86	0.40	
C-Reaction Time	173.91	1	173.91	0.62	0.47	
AB	24.90	1	24.90	0.09	0.78	
AC	6.73	1	6.73	0.02	0.88	
BC	39.00	1	39.00	0.14	0.73	
A^2	368.86	1	368.86	1.31	0.30	
B^2	42.05	1	42.06	0.15	0.72	
C^2	214.53	1	214.53	0.76	0.42	
Residual	1407.77	5	281.55			
Lack of Fit	1387.01	3	462.34	44.55	0.02	significant
Pure Error	20.76	2	10.38			
Cor Total	2562.53	14				
R^2 = 0.4506	Adjusted R^2 = -0.5382	Predicted R^2 = -7.6785		Adeq-Precision = 1.9947		

For each dependent variable, a quadratic model was defined to characterize the main and interaction effects of factors within the RSM framework. Design-Expert software was employed for model selection, assessment of adequacy, and generation of optimization plots. The appropriateness of model statistical evaluation was conducted.

Table 5. ANOVA test for the yield of phenolic compounds using the quadratic response surface model

Source	Sum of squares	Degree of freedom	Mean square	F-value	p-value	Significance
Model	142.01	9	15.78	1.83	0.26	not significant
A-Co Ratio	3.33	1	3.33	0.39	0.56	
B-Temperature	6.53	1	6.53	0.76	0.42	
C-Reaction Time	13.34	1	13.34	1.54	0.27	
AB	61.47	1	61.47	7.11	0.04	
AC	9.49	1	9.49	1.10	0.34	
BC	2.48	1	2.48	0.29	0.62	
A^2	35.55	1	35.55	4.11	0.10	
B^2	12.44	1	12.44	1.44	0.28	
C^2	0.01	1	0.01	0.00	0.98	
Residual	43.20	5	8.64			
Lack of Fit	43.08	3	14.36	250.06	0.01	significant
Pure Error	0.11	2	0.06			
Cor Total	185.21	14				
R^2 = 0.7667	Adjusted R^2 = -0.3469	Predicted R^2 = -2.7235		Adeq-Precision = 4.2578		

The ANOVA results for the polynomial response surface models indicated a significant Lack of Fit for both the vanillin (P=0.02) and phenolic (P=0.01) models. The coefficient of determination (R^2) for vanillin yield was 0.4506 and 0.7667 for phenolic compound yield, with corresponding adjusted R^2 values of -0.5382 and -0.3469. These low R^2 and negative adjusted R^2 values, coupled with the significant Lack of Fit, collectively indicate that the applied quadratic model may not fully capture the complex relationships governing vanillin and phenolic yields, thus limiting its accuracy for precise prediction. Multiple regression analysis using Design-Expert software was performed to determine the coefficients of the regression equations. The determination of optimal points was facilitated by solving the second-degree multivariable equations. Based on the regression analysis results, the derived coefficients can be utilized for predicting vanillin and phenolic compound yields. The specific empirical quadratic equations are:

$$X_{\text{Vanillin yield (\%)}} = 16.22 - 3.68A - 5.5B - 4.66C + 2.49AB - 1.3AC - 3.12BC + 10A^2 + 3.38B^2 + 7.63C^2 \quad \text{(Eq. 2)}$$

Three-dimensional response surface plots (Figure 4a-b right-hand side) illustrate the predicted versus actual yields, where color gradients indicate yield levels (red for high, green for medium, blue for low) (Buenaño et al., 2024). Analysis of the model coefficients revealed that the interaction between the Co:Mo ratio (Factor A) and Temperature (Factor B) exerted the strongest impact on both responses. For the Co:Mo ratio, linear terms exhibited negative coefficients while corresponding quadratic terms were positive, indicating an initial yield decrease followed by a drastic increase beyond a certain threshold. This non-linear behavior suggests that an optimal Co:Mo ratio exists, where a balance between active site availability and potential mass transfer limitations or phase segregation might be crucial. Based on the analysis conducted with DesignExpert software, the optimal parameters for the reaction of BPE to vanillin and phenolic compounds, particularly for potential industrial-scale application, were determined to be a Co:Mo ratio of 3:7, a temperature of 169 °C, and a reaction time of 31 minutes.

$$X_{\text{Phenolic yield (\%)}} = 0.32 - 0.64A + 0.9B + 1.29C + 3.92AB - 1.54AC - 0.78BC + 3.1A^2 + 1.83B^2 + 0.04C^2 \quad \text{(Eq. 3)}$$

In addition to the mentioned criteria for evaluating model accuracy, the difference between predicted and experimental responses (residuals) was graphically utilized to assess model precision. Residuals represent deviations not captured by the model. The predicted values versus the actual values of the studied variables for the conversion of BPE are presented in Figure 4a-b on the left. As observed, there is no sufficient agreement between the actual data and the model-derived data, suggesting that the quadratic model might not adequately capture the complex relationship governing vanillin yield, and other unmeasured factors or a more complex kinetic pathway might be influencing its production.

Regarding Reaction Time (Factor C), a negative correlation was observed with % yield vanillin, while a small positive correlation was found with % yield phenolic compounds. The observed decrease in vanillin concentration at longer reaction times suggests its further conversion. This is supported by HPLC analysis, which revealed new peaks at retention times distinct from vanillin or phenol. This phenomenon is consistent with literature reports, where vanillin can undergo further hydrogenation and hydrodeoxygenation reactions, potentially yielding compounds such as vanillyl alcohol, 4-(dimethoxymethyl)-2-methoxyphenol, 2-methoxy-4-(methoxymethyl) phenol, and cresol.

The reaction mechanism for the conversion of BPE to phenol and vanillin is proposed to proceed via a multi-step reaction mechanism (Fig. S2). The initial step involves the cleavage of the ether (C–O) bond in BPE, forming smaller fragments that subsequently diffuse into the zeolite pores. This ether bond scission is catalyzed by the acidic sites (H^+) present on the H-ZSM-5 surface, where BPE undergoes protonation, leading to the breaking of the ether linkage and the formation of phenol and a benzyl cation.

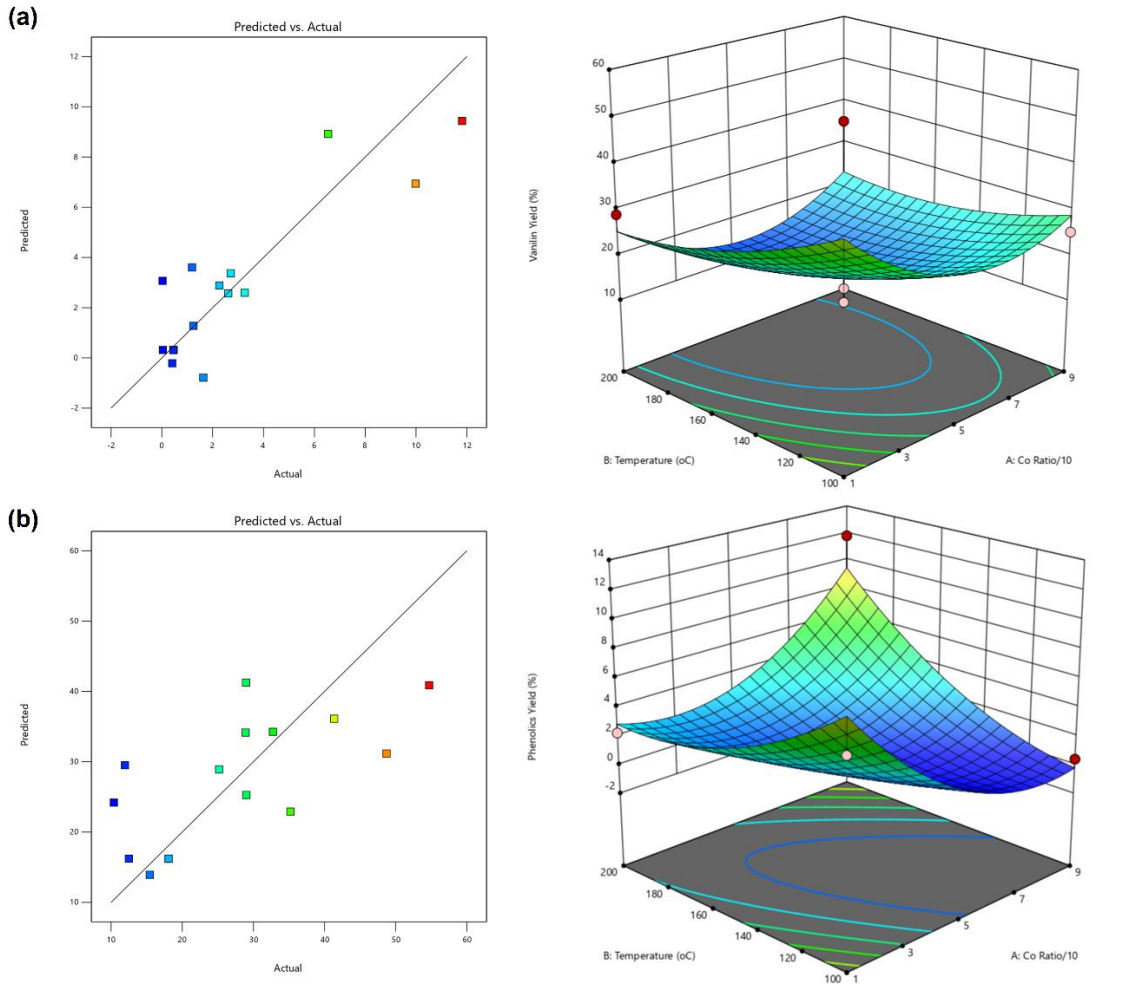

Fig. 4. Two-dimensional (2D) predicted vs actual plot (left) and three-dimensional (3D) response surface plot (right) for (a) vanillin yield (%); (b) phenolic compounds yield (%)

The benzyl cation is then presumed to deprotonate water, yielding benzyl alcohol. Following the initial ether cleavage, the generated phenol diffuses into the H-ZSM-5 pores. Here, the bimetallic CoMo oxides, whose successful incorporation and phase distribution were confirmed by XRD (Figure 1a) and FTIR (Figure 1b), are hypothesized to act as oxidizers, converting phenol into vanillin. The specific phases identified by XRD ($CoMoO_4$, Co_3O_4, MoO_3) likely contribute differently to the overall catalytic activity and selectivity. The decrease in total surface area (S_{BET}) upon metal impregnation (Table 2) suggests potential pore blockage, which could affect substrate diffusion. However, the presence of various bimetallic oxide species with varying dispersion levels (as indicated by SEM and EDS mapping analyses in Figure 2, and Figure 3) plays a crucial role in the catalytic performance. The hierarchical structure of H-ZSM-5 itself, with its combination of micropores and mesopores, is essential for facilitating efficient mass transport of bulky molecules like BPE and its products, thus enhancing access to the active sites located within the zeolite framework and on the dispersed metal oxide species.

4. Conclusions

This study successfully synthesized hierarchical H-Z via a dual-template method, which was subsequently impregnated with bimetallic Co-Mo oxides for the catalytic conversion of benzyl phenyl ether to vanillin and phenol. Catalyst characterization confirmed the successful preparation and modification. TIR analysis confirmed the complete removal of organic templates after calcination, while XRD confirmed the preservation of the characteristic ZSM-5 framework even after bimetal CoMo oxide impregnation, validating

the structural integrity of the catalyst. Catalytic activity tests demonstrated 100% BPE conversion, with the highest vanillin product yield recorded at 54.69%, achieved when utilizing a 1:9 Co:Mo ratio (1Co9Mo/H-Z) at 150 °C for 30 minutes. The Box-Behnken design effectively elucidated the influence of varying Co ratio, temperature, and reaction time on the BPE conversion to vanillin and phenolic compounds. The optimization study revealed that the interaction between the Co:Mo ratio and temperature exerted the greatest influence compared to other interaction factors. Furthermore, the Co ratio demonstrated the largest quadratic impact on both vanillin and phenol yields. Based on the analysis conducted with DesignExpert software, the optimal parameters for the reaction of BPE to vanillin and phenolic compounds, particularly for potential industrial-scale application, were determined to be a Co:Mo ratio of 3:7, at temperature of 169 °C, and a reaction time of 31 minutes. These findings provide crucial insights into the efficient production of high-value chemicals from lignin model compounds using a hierarchically structured bimetallic zeolite catalyst.

Acknowledgement
The authors gratefully acknowledge the support, guidance, and contributions that were essential to the completion of this work.

Author Contribution
Conceptualization, Y.K.K. and R.F.H.; Methodology, Y.K.K. and R.W.; Validation, D.R.A. and I.K.; Formal Analysis, D.R.A.; Investigation, D.R.A.; Data Curation, D.R.A. and I.K.; Writing – Original Draft Preparation, I.K.; Writing – Review & Editing, I.K. and Y.K.K.; Visualization, I.K.; Supervision, Y.K.K. and R.W.; Project Administration, Y.K.K.; and Funding Acquisition, Y.K.K.

Funding
Universitas Indonesia funded this research through Hibah Publikasi Terindeks Internasional (PUTI) Q2 Research Grant No. NKB-670/UN2.RST/HKP.05.00/2022.

Ethical Review Board Statement
Not available.

Informed Consent Statement
Not available.

Appendix A. Supplementary Data
Supplementary data to this article can be found online at
https://drive.google.com/drive/folders/14Tt2ZgrKaui67JT89YsKOcNoBCersowh

Data Availability Statement
Not available.

Conflicts of Interest
The authors declare no conflict of interest.

References

Ahmad, K., & Upadhyayula, S. (2019). Conversion of the greenhouse gas CO_2 to methanol over supported intermetallic Ga–Ni catalysts at atmospheric pressure: thermodynamic modeling and experimental study. *Sustainable Energy & Fuels*, *3*(9), 2509–2520. https://doi.org/10.1039/C9SE00165D

Al-Jubouri, S. M. (2020). Synthesis of hierarchically porous ZSM-5 zeolite by self-assembly induced by aging in the absence of seeding-assistance. *Microporous and Mesoporous Materials*, *303*, 110296. https://doi.org/10.1016/J.MICROMESO.2020.110296

Asghar, A., Iqbal, N., Aftab, L., Noor, T., Kariuki, B. M., Kidwell, L., & Easun, T. L. (2020). Ethylenediamine loading into a manganese-based metal–organic framework enhances water stability and carbon dioxide uptake of the framework. *Royal Society Open Science*, *7*(3). https://doi.org/10.1098/RSOS.191934

Azreena, I. N., Lau, H. L. N., Asikin-Mijan, N., Hassan, M. A., Izham, S. M., Kennedy, E., ... & Taufiq-Yap, Y. H. (2021). A promoter effect on hydrodeoxygenation reactions of oleic acid by zeolite beta catalysts. *Journal of analytical and applied pyrolysis*, *155*, 105044. https://doi.org/10.1016/J.JAAP.2021.105044

Bakhtyari, A., Rahimpour, M. R., & Raeissi, S. (2020). Cobalt-molybdenum catalysts for the hydrodeoxygenation of cyclohexanone. *Renewable Energy*, *150*, 443–455. https://doi.org/10.1016/J.RENENE.2019.12.119

Bakhtyari, A., Sakhayi, A., Rahimpour, M. R., & Iulianelli, A. (2024). Conversion of lignin-derived ketonic intermediate to biofuel products: Syngas-assisted vs. Conventional hydrotreating. *Fuel Processing Technology*, *256*, 108077. https://doi.org/10.1016/J.FUPROC.2024.108077

Bezerra, M. A., Santelli, R. E., Oliveira, E. P., Villar, L. S., & Escaleira, L. A. (2008). Response surface methodology (RSM) as a tool for optimization in analytical chemistry. *Talanta*, *76*(5), 965–977. https://doi.org/10.1016/J.TALANTA.2008.05.019

Buenaño, L., Ali, E., Jafer, A., Zaki, S. H., Hammady, F. J., Khayoun Alsaadi, S. B., ... & Kazemi, A. (2024). Optimization by Box–Behnken design for environmental contaminants removal using magnetic nanocomposite. *Scientific Reports*, *14*(1), 6950. https://doi.org/10.1038/S41598-024-57616-8

Dwivedi, G., & Sharma, M. P. (2015). Application of Box–Behnken design in optimization of biodiesel yield from Pongamia oil and its stability analysis. *Fuel*, *145*, 256–262. https://doi.org/10.1016/J.FUEL.2014.12.063

El-Sheekh, M., Alwaleed, E. A., Kassem, W. M. A., & Saber, H. (2024). Optimizing the fucoidan extraction using Box-Behnken design and its potential bioactivity. *International Journal of Biological Macromolecules*, *277*, 134490. https://doi.org/10.1016/J.IJBIOMAC.2024.134490

Fan, C., Wu, Z., Li, Z., Qin, Z., Zhu, H., Dong, M., Wang, J., & Fan, W. (2023). Controllable preparation of ultrafine Co3O4 nanoparticles on H-ZSM-5 with superior catalytic performance in lean methane combustion. *Fuel*, *334*, 126815. https://doi.org/10.1016/J.FUEL.2022.126815

Gamal, M. S., Asikin-Mijan, N., Khalit, W. N. A. W., Arumugam, M., Izham, S. M., & Taufiq-Yap, Y. H. (2020). Effective catalytic deoxygenation of palm fatty acid distillate for green diesel production under hydrogen-free atmosphere over bimetallic catalyst CoMo supported on activated carbon. *Fuel Processing Technology*, *208*, 106519. https://doi.org/10.1016/J.FUPROC.2020.106519

Gille, T., Seifert, M., Marschall, M. S., Bredow, S., Schneider, T., Busse, O., Reschetilowski, W., & Weigand, J. J. (2021). Conversion of Oxygenates on H-ZSM-5 Zeolites—Effects of Feed Structure and Si/Al Ratio on the Product Quality. *Catalysts*, *11*(4), 432. https://doi.org/10.3390/CATAL11040432

Jiang, W., Cao, J. P., Yang, Z., Xie, J. X., Zhao, L., Zhu, C., Zhang, C., Zhao, X. Y., Zhao, Y. P., & Zhang, J. L. (2022). Hydrodeoxygenation of lignin and its model compounds to hydrocarbon fuels over a bifunctional Ga-doped HZSM-5 supported metal Ru catalyst. *Applied Catalysis A: General*, *633*, 118516. https://doi.org/10.1016/J.APCATA.2022.118516

Keluo, C. H. E. N., Zhang, T., Xiaohui, C. H. E. N., Yingjie, H. E., & Liang, X. (2018). Model construction of micro-pores in shale: A case study of Silurian Longmaxi Formation shale in Dianqianbei area, SW China. *Petroleum Exploration and Development*, *45*(3), 412-421. https://doi.org/10.1016/S1876-3804(18)30046-6

Kohler, A. J., Walter, C. H., & Shanks, B. H. (2023). Kinetic Analysis of the Hydrodeoxygenation of Aliphatic Volatilized Lignin Molecules on Bulk MoO3: Elucidating the Formation of Alkenes and Alkanes. *ACS Catalysis*, *13*(22), 14813–14827. https://pubs.acs.org/doi/abs/10.1021/acscatal.3c04444

Kostyniuk, A., Key, D., & Mdleleni, M. (2020). 1-hexene isomerization over bimetallic M-Mo-ZSM-5 (M: Fe, Co, Ni) zeolite catalysts: Effects of transition metals addition on the catalytic performance. *Journal of the Energy Institute*, *93*(2), 552–564. https://doi.org/10.1016/J.JOEI.2019.06.009

Kramer, C. A. C., & De Carvalho, L. S. (2021). α-Oxidation of banana lignin with atmospheric oxygen catalyzed by Co3O4. *Reaction Chemistry & Engineering*, *6*(6), 1016–1022. https://doi.org/10.1039/D1RE00053E

Kumar, A., Prasad, R., & Sharma, Y. C. (2019). Ethanol steam reforming study over ZSM-5 supported cobalt versus nickel catalyst for renewable hydrogen generation. *Chinese Journal of Chemical Engineering*, *27*(3), 677–684. https://doi.org/10.1016/J.CJCHE.2018.03.036

Liu, C. F., He, L. C., Wang, X. F., Chen, J., Lu, J. Q., & Luo, M. F. (2022). Tailoring Co3O4 active species to promote propane combustion over Co3O4/ZSM-5 catalyst. *Molecular Catalysis*, *524*, 112297. https://doi.org/10.1016/J.MCAT.2022.112297

Luo, W., Cao, W., Bruijnincx, P. C. A., Lin, L., Wang, A., & Zhang, T. (2019). Zeolite-supported metal catalysts for selective hydrodeoxygenation of biomass-derived platform molecules. *Green Chemistry*, *21*(14), 3744–3768. https://doi.org/10.1039/C9GC01216H

Luo, W., Yang, X., Wang, Z., Huang, W., Chen, J., Jiang, W., Wang, L., Cheng, X., Deng, Y., & Zhao, D. (2017). Synthesis of ZSM-5 aggregates made of zeolite nanocrystals through a simple solvent-free method. *Microporous and Mesoporous Materials*, *243*, 112–118. https://doi.org/10.1016/J.MICROMESO.2017.01.040

Mate, V. R., Jha, A., Joshi, U. D., Patil, K. R., Shirai, M., & Rode, C. V. (2014). Effect of preparation parameters on characterization and activity of Co3O4 catalyst in liquid phase oxidation of lignin model substrates. *Applied Catalysis A: General*, *487*, 130–138. https://doi.org/10.1016/J.APCATA.2014.08.023

Min, J. E., Kim, S., Kwak, G., Kim, Y. T., Han, S. J., Lee, Y., Jun, K. W., & Kim, S. K. (2018). Role of mesopores in Co/ZSM-5 for the direct synthesis of liquid fuel by Fischer–Tropsch synthesis. *Catalysis Science & Technology*, *8*(24), 6346–6359. https://doi.org/10.1039/C8CY01931B

Moravvej, Z., Farshchi Tabrizi, F., Rahimpour, M. R., & Behrad Vakylabad, A. (2023). Exploiting the potential of cobalt molybdenum catalyst in elevated hydrodeoxygenation of furfural to 2-methyl furan. *Fuel*, *332*, 126193. https://doi.org/10.1016/J.FUEL.2022.126193

Nada, M. H., & Larsen, S. C. (2017). Insight into seed-assisted template free synthesis of ZSM-5 zeolites. *Microporous and Mesoporous Materials*, *239*, 444–452. https://doi.org/10.1016/J.MICROMESO.2016.10.040

Nazari, M., Yaripour, F., & Shifteh, S. (2021). Systematic evaluation and optimization of crystallization conditions for an ethanol-templated ZSM-5 zeolite using response surface methodology. *Advanced Powder Technology*, *32*(12), 4621–4634. https://doi.org/10.1016/j.apt.2021.10.018

Pan, L., Wu, S., Huang, Z., Zhang, S., Wang, L., & Zhang, J. (2022). MoO 3 -modified SAPO-34 for photocatalytic nonoxidative coupling of methane. *Catalysis Science & Technology*, *12*(10), 3322–3327. https://doi.org/10.1039/D2CY00502F

Prasad, K., Mahato, N., Yoo, K., & Kim, J. (2023). Morphology Regulated Hierarchical Rods-, Buds-, and Sheets-like CoMoO4 for Electrocatalytic Oxygen Evolution Reaction. *Energies 2023, Vol. 16, Page 2441*, *16*(5), 2441. https://doi.org/10.3390/EN16052441

Pratama, A. P., Rahayu, D. U. C., & Krisnandi, Y. K. (2020). Levulinic acid production from delignified rice husk waste over manganese catalysts: Heterogeneous versus homogeneous. *Catalysts*, *10*(3). https://doi.org/10.3390/catal10030327

Ramadhani, A. N., Abdullah, I., & Krisnandi, Y. K. (2022). Effect of Physicochemical Properties of Co and Mo Modified Natural Sourced Hierarchical ZSM-5 Zeolite Catalysts on Vanillin and Phenol Production from Diphenyl Ether. *Bulletin of Chemical Reaction Engineering & Catalysis*, *17*(1), 225–239. https://doi.org/10.9767/BCREC.17.1.13372.225-239

Sabarish, R., & Unnikrishnan, G. (2017). Synthesis, characterization and catalytic activity of hierarchical ZSM-5 templated by carboxymethyl cellulose. *Powder Technology*, *320*, 412–419. https://doi.org/10.1016/J.POWTEC.2017.07.041

Saini, K., Kumar, A., Biswas, B., & Bhaskar, T. (2022). Low-temperature alkali lignin depolymerization to functional chemicals. *Biomass Conversion and Biorefinery*, *12*(1), 209–219. https://doi.org/10.1007/S13399-021-01478-X/METRICS

Serrano, D. P., Pinnavaia, T. J., Aguado, J., Escola, J. M., Peral, A., & Villalba, L. (2014). Hierarchical ZSM-5 zeolites synthesized by silanization of protozeolitic units: Mediating the mesoporosity contribution by changing the organosilane type. *Catalysis Today*, *227*, 15–25. https://doi.org/10.1016/J.CATTOD.2013.10.052

Song, S., Zhang, J., & Yan, N. (2020). Support effects in the de-methoxylation of lignin monomer 4-propylguaiacol over molybdenum-based catalysts. *Fuel Processing Technology*, *199*, 106224. https://doi.org/10.1016/J.FUPROC.2019.106224

Syeitkhajy, A., Hamid, M. A., Boroglu, M. S., & Boz, I. (2025). Efficient synthesis of phosphorus-promoted and alkali-modified ZSM-5 catalyst for catalytic dehydration of lactic acid to acrylic acid. *Results in Chemistry*, *13*, 101942. https://doi.org/10.1016/J.RECHEM.2024.101942

Treacy, M. M. J., & Higgins, J. B. (2007). ZSM-5, Calcined. *Collection of Simulated XRD Powder Patterns for Zeolites*, 278–279. https://doi.org/10.1016/B978-044453067-7/50604-3

Wang, B., Yang, X., Chen, Y., Wang, J., Lan, M., Tang, K., & Yang, F. (2024). Biomass-Derived-Carbon-Supported Spinel Cobalt Molybdate as High-Efficiency Electrocatalyst for Oxygen Evolution Reaction. *Molecules*, *29*(20), 4953. https://doi.org/10.3390/MOLECULES29204953/S1

Wang, L., Zhang, Z., Yin, C., Shan, Z., & Xiao, F. S. (2010). Hierarchical mesoporous zeolites with controllable mesoporosity templated from cationic polymers. *Microporous and Mesoporous Materials*, *131*(1–3), 58–67. https://doi.org/10.1016/j.micromeso.2009.12.001

Zeng, H., Cao, D., Qiu, Z., & Li, C.-J. (2018). Palladium-Catalyzed Formal Cross-Coupling of Diaryl Ethers with Amines: Slicing the 4-O-5 Linkage in Lignin Models. *Angewandte Chemie*, *130*(14), 3814–3819. https://doi.org/10.1002/ANGE.201712211

Zhao, J., Jayakumar, A., & Lee, J. M. (2018). Bifunctional Sulfonated MoO3-ZrO2 Binary Oxide Catalysts for the One-Step Synthesis of 2,5-Diformylfuran from Fructose. *ACS Sustainable Chemistry and Engineering*, *6*(3), 2976–2982. https://pubs.acs.org/doi/abs/10.1021/acssuschemeng.7b02671

Zhu, Z., Lu, G., Zhang, Z., Guo, Y., Guo, Y., & Wang, Y. (2013). Highly active and stable Co3O4/ZSM-5 catalyst for propane oxidation: Effect of the preparation method. *ACS Catalysis*, *3*(6), 1154–1164. https://doi.org/10.1021/CS400068V

Biographies of Authors

Irena Khatrin, Department of Chemistry, Faculty of Mathematics and Natural Science, Universitas Indonesia, Depok, West Java 16424, Indonesia.
- Email: irena.khatrin@sci.ui.ac.id
- ORCID: 0000-0002-3490-0643
- Web of Science ResearcherID: N/A
- Scopus Author ID: 58077997600
- Homepage: https://scholar.google.com/citations?user=U-DKnUUAAAAJ&hl=en

Duha Rushida Amanullah, Department of Chemistry, Faculty of Mathematics and Natural Science, Universitas Indonesia, Depok, West Java 16424, Indonesia.
- Email: duha.rushida@ui.ac.id
- ORCID: N/A
- Web of Science ResearcherID: N/A
- Scopus Author ID: N/A
- Homepage: N/A

Rahmat Wibowo, Department of Chemistry, Faculty of Mathematics and Natural Science, Universitas Indonesia, Depok, West Java 16424, Indonesia.
- Email: rahmat.wibowo@sci.ui.ac.id
- ORCID: 0000-0001-5431-4548
- Web of Science ResearcherID: N/A
- Scopus Author ID: 57200846522
- Homepage: https://scholar.google.com/citations?user=kUHS48QAAAAJ&hl=id

Russell Francis Howe, Department of Chemistry, School of Natural and Computing Sciences, University of Aberdeen, Aberdeen, Scotland AB24 3UE, United Kingdom.
- Email: r.howe@abdn.ac.uk
- ORCID: 0000-0003-2462-8962
- Web of Science ResearcherID: N/A
- Scopus Author ID: 57188675863
- Homepage: N/A

Yuni Krisyuningsih Krisnandi, Department of Chemistry, Faculty of Mathematics and Natural Science, Universitas Indonesia, Depok, West Java 16424, Indonesia.
- Email: yuni.krisnandi@sci.ui.ac.id
- ORCID: 0000-0002-2753-5596
- Web of Science ResearcherID: N/A
- Scopus Author ID: 12761423100
- Homepage: https://scholar.ui.ac.id/en/persons/yuni-krisyuningsih